International Journal of Pharmaceutics 411 (2011) 49–63

Contents lists available at ScienceDirect

International Journal of Pharmaceutics

journal homepage: www.elsevier.com/locate/ijpharm

The breakage behaviour of Aspirin under quasi-static indentation and single particle impact loading: Effect of crystallographic anisotropy

D. Olusanmi*, K.J. Roberts, M. Ghadiri, Y. Ding

Institute of Particle Science and Engineering, School of Process, Environmental and Materials Engineering, University of Leeds, Leeds LS2 9JT, United Kingdom

ARTICLE INFO

Article history:
Received 17 January 2011
Accepted 18 March 2011
Available online 3 April 2011

Keywords:
Milling
Impact
Nano-indentation
Cleavage
Aspirin
Breakage

ABSTRACT

The influence of crystallographic structural anisotropy on the breakage behaviour of Aspirin under impact loading is highlighted. Under both quasi-static testing conditions, using nano-indentation, and dynamic impact tests, Aspirin demonstrates clear anisotropy in its slip and fracture behaviour. During nano-indentation on the (1 0 0) and (0 0 1) faces, cracks were propagated along the [0 1 0] direction. While the hardness was found to be comparatively similar for both these faces, it was observed that slip due to plastic deformation occurred more readily on the (1 0 0) than the (0 0 1) crystal planes suggesting the former as the preferred slip plane. Furthermore, the fracture toughness on the (0 0 1) planes was found to be distinctly lower than that of the (1 0 0) planes, indicating the former as the preferred cleavage plane. Observations of the crystal morphology of damaged particles after dynamic impact testing showed that both the chipping and fragmentation of Aspirin mostly occurred via cleavage in a manner consistent with the observed fracture behaviour following nano-indentation. This work highlights the importance of cleavage as a dominant factor underpinning the fracture mechanism of Aspirin under both quasi-static and impact loading conditions.

1. Introduction

Milling is an important unit operation which forms a key part during the processing of particulate solids in many industries including the chemical, food, mining, pigment and ink manufacturing, and pharmaceutical industries. The aims of milling are to reduce the size of particles for enhanced product properties including dissolution and dispersion, to increase surface area of particles needed for reactions, or to obtain an immediate product for mixing with other materials to form multifunctional composite particulate products. In the pharmaceutical industry, the majority of drug active ingredients are produced by crystallisation from solution; however, they are rarely used in their crystallised size. The requirement for content uniformity, especially for low dose active pharmaceutical ingredient (API) drug loadings often makes milling a necessity. More crucially, the dissolution of pharmaceutical drugs may be improved by increased surface area facilitated by milling. However, the lack of a systematic and scientific approach towards understanding and hence controlling milling processes has the potential to lead to the production of excessively fine particulates, and a wide particle size distribution beyond what might be required and/or might display physical property characteristics, e.g. increased amorphous content, change in hydrate/solvate state or formation of powders which are outside the range of the specification needed in formulation. These factors coupled with the potential for particles to exhibit electrostatic charging may further complicate powder handing problems such as cohesivity, aggregation, poor flowability and stickiness of API powders downstream of milling thereby impacting on processes such as blending, granulation and compaction. To enable a much better understanding and control of milling processes material properties characterised at the single particle level can be used as an indication of bulk milling behaviour (Kwan et al., 2004). This has been demonstrated successfully by Taylor et al. (2004a), who carried out nano-indentation on a number of pharmaceutical particulates and observed a good correlation between the results from these tests and large scale pilot-plant mills, this despite the differences in relative strain rates of the two processes. For materials which are strain rate sensitive mechanical properties characterised at low strain rates such as during nano-indentation might not always apply at the higher strain rates prevailing during milling. Generally material properties such as hardness, Young's modulus and fracture toughness, which are known to influence the breakage behaviour of materials, were previously inferred from compacted specimens (Kerridge and Newton, 1986; Mashadi and Newton, 1988; Roberts and Rowe, 1989, 1996; York et al., 1990; Bassam et al., 1990; Roberts et al., 1991; Rodford et al., 1993) or determined by indentation on single crystals (Ridgway et al., 1969;

* Corresponding author. Tel.: +44 0 1516042004; fax: +44 0 1515521615.
E-mail address: dolapo.olusanmi@bms.com (D. Olusanmi).

0378-5173/$ – see front matter © 2011 Elsevier B.V. All rights reserved.
doi:10.1016/j.ijpharm.2011.03.039

Nomenclature

a	constant in Eq. (2) (kg/s^2)
B	Burgers' vector (Å)
E	Young's modulus (GPa)
E_{core}	core energy of a dislocation (J)
E_d	dislocation energy (J)
E_{line}	line energy of a dislocation (J)
E_r	reduced modulus (GPa)
f_{Mat}	material parameters in Eq. (6) (kg/J m)
$(h\,k\,l)$	Miller indices (Å)
H	hardness (GPa)
l	particle size (μm)
k	number of impacts (in Eq. (6))
K_c	critical stress intensity factor (MPa m$^{1/2}$)
M_{de}	mass of debris particles (g)
M_f	mass of feed particles (g)
M_m	mass of mother particles (g)
R^*	breakage propensity (%)
$[u\,v\,w]$	directional indices of dislocation Burgers' vector
R^2	regression coefficient
S_b	breakage probability in Eq. (6)
v	impact velocity (m/s)
$W_{m,kin}$	kinetic impact energy (J/kg)
$W_{m,min}$	threshold energy for particle breakage (J/kg)
x_b	Berkovich indenter constant
x_v	Vickers indenter constant

Duncan-Hewitt and Weatherly, 1989a,b; Arteaga et al., 1993; Taylor et al., 2004b; Meier et al., 2009). The aforementioned mechanical properties and in particular their inter-relationships provide important information on the breakage behaviour of particulate materials: the ratio of hardness (H) to fracture toughness (K_c), H/K_c, is an empirical relation which has been suggested by Lawn and Marshall, 1979 as a 'Brittleness Index' which can be used to rank materials in order of their brittleness. More recently Ghadiri and Zhang (2002) have developed an impact breakage model for semi-brittle solids, where the ratio H/K_c^2 has been shown to describe the breakage propensity of materials tested under single impact loading conditions. However, depending on their crystallographic structure the mechanical properties of organic crystalline materials may exhibit highly anisotropic behaviour with respect to the crystal chemistry. With regard to predicting the breakage behaviour of particulate materials under impact loading, it is important to note their mechanical property anisotropy, and the planes on which mechanical deformation measurements are generated needs to be considered as fracture can be expected to propagate more readily on low energy cleavage planes. This therefore has implications on prevalence of certain crystallographic planes in the processed product with potential consequences on surface energetics, dissolution rate, cohesion, etc. The objective of this paper is to highlight the role of this mechanical property anisotropy on the deformation and breakage behaviour of a representative organic molecular material, Aspirin.

The structure of this paper is as follows. After this, the introduction, an overview of the mechanical deformation of organic solids is given, followed by literature review on the determination of mechanical properties of organic materials highlighting some of the factors which might affect mechanical deformation studies. Details of the material used and experimental methodology adopted is then provided followed by the associated experimental results. This is then rationalised with respect to the literature and conclusions drawn.

2. Mechanical deformation of organic solids

2.1. Theoretical considerations

Organic materials mostly crystallise in low symmetry structures, typically triclinic, monoclinic and orthorhombic (Cambridge Crystallographic Data Centre, CCDC). The rather weak intermolecular forces (mostly van der Waals interactions and hydrogen bonding) inherent for such materials can give rise to comparatively soft materials. In contrast to elemental compounds, the mechanical deformation properties of such materials can often be highly anisotropic, reflecting a number of factors including anisotropy in molecular structure, elastic constants, dislocation Burgers' vector $[u\,v\,w]$ and available slip planes $(h\,k\,l)$. The latter two factors exhibit a much lower multiplicity in organic crystals due to lower crystal symmetry than for simple elemental systems.

Crystal deformation under mechanical stress takes place elastically initially and then plastically. The latter process is usually expected to take place on low index (h, k, l <2) slip planes (Hirth and Lothe, 1982). Such planes can usually be identified by two main factors. Firstly, lattice planes which have a higher in-plane molecular density and concomitant weak inter-planar interaction will permit interplanar movement under the influence of shearing forces. In this case, the surface energy is a useful measure of the ease with which a given plane will slip. Secondly, lattice planes that exhibit lower molecular-scale rugosity will allow two adjacent surfaces to pass over each other without a significant energy barrier due to repulsive steric interactions between the passing molecules. In contrast, crystal planes characterized by an interlocking molecular packing structure may find slip impossible, even when the surface energies are quite low.

Plastic deformation requires dislocation motion along the low index slip planes subject to the requirement:

$$hu + kv + lw = 0 \tag{1}$$

where $(h\,k\,l)$ is the Miller index of the slip plane and $[u\,v\,w]$ is the directional index associated with the lattice direction of the dislocation Burgers' vector, $\underline{b}$.

The formation energy, E_d, of a dislocation is a combination of the core and the line energies and can be given as

$$E_d = E_{line}(\text{elastic}) + E_{core}(\text{inelastic}) \tag{2}$$

where the former term dominates and so the approximation in Eq. (3) below is valid.

$$E_d \approx E_{line} \tag{3}$$

E_{line} reflects the stored elastic energy due to the defect which is given by:

$$E_{line}^{(screw)} = cG\left|\underline{b}\right|^2 \tag{4}$$

for a screw dislocation and

$$E_{line}^{(edge)} = \frac{E_{line}^{(screw)}}{1-\nu} \tag{5}$$

for an edge dislocation. where c is a constant which reflects the extent of the strain field around the dislocation, $|\underline{b}|$ is the magnitude of the Burgers' vector, and G and ν are the bulk modulus and Poisson's ratio, respectively. Caution is needed in over-interpreting the absolute values of these energies mindful that for anisotropic systems the full elastic tensor is needed to define these quantitatively. Nonetheless, in terms of relative energies, the shortest Burgers' vectors have the lowest energy and are therefore the most likely to dominate the landscape of plastic deformation. An interesting characteristic of the crystallography of organic crystals is that the requirement for low rugosity surfaces and short Burgers' vectors

is often not met together, i.e. the shortest intermolecular distances are often perpendicular to the slip plane surface due to the effect of the molecules in organic materials not being spherical. Thus, for example low energy dislocations may not be able to slip at the most theoretically preferred slip planes.

The transformation from elastic to plastic behaviour reflects the activation energy barrier associated with formation of the dislocation slip systems. Crystal fracture takes place when the shear stress reaches a level where dislocation pile-up attains a critical density. Some materials can also fracture along specific crystal planes by cleavage where the surface energy is very low. Following sustained plastic deformation dislocations active on different slip planes can, in principle, intersect and lock together and, through this, restrict further ductile behaviour. This well-known process of work hardening can lead eventually to crystal fracture below the expected intrinsic brittle fracture limit. Due to the lower multiplicity for the Burgers vectors and slip planes for organic materials one might expect less work hardening when compared to elemental compounds such as metals (Hirth and Lothe, 1982) but experimental studies probing this aspect are not very common.

The dominant features inherent in the mechanical deformation of organic crystals can thus be summarized:

- Strong molecular and crystallographic anisotropy reflecting complex molecular shape together with low symmetry crystal structures.
- Mostly, weak intermolecular forces giving rise to low values of the elastic moduli resulting in soft materials.
- Slip planes characterised by low surface energy and rugosity.
- Plastic deformation restricted by low slip plane and Burgers' vector multiplicity and limited combinations of these two to create active slip systems.
- Fracture behaviour giving rise to either brittle or semi-brittle fracture behaviour depending on the activation energies of the various plastic deformation slip systems, with fracture by cleavage also taking place when the surface rugosity and surface energy is very low.

In this paper the relevance of the above features to deformation and fracture of organic crystals is explored through careful indentation on Aspirin crystals.

2.2. Overview of literature on the characterisation of mechanical properties of organic molecular particulates

Characterisation of the mechanical properties of fine particulate materials is difficult to carry out due to their small size. In the past powders have been compacted to different porosities to prepare specimens for mechanical testing. Using different mechanical characterisation techniques described by Rowe and Roberts (1996), mechanical properties such as hardness, Young's modulus and fracture toughness have previously been determined from compacted specimens, and the properties of single particles have been inferred by extrapolating the values obtained at different compact porosities to zero porosity.

Several factors could affect the results of mechanical properties obtained from compacted specimens, thereby introducing significant uncertainties in the validity of these measurements such that they cannot be used with confidence. The preparation of compacted specimens at different porosities requires a significant amount of material, which is most undesirable especially in the pharmaceutical industry during the early stages of drug development. The use of compacted specimens is based on the assumption that random particle orientations are present in a powder compact and gives an averaged picture of the material mechanical properties. This might not be the case. Furthermore, the formation of these compacts at different porosities assumes uniform porosity throughout the compact. The uniform porosity assumption might not hold true due to non-uniform distribution of force/stress within the powder. In addition, the formation of a compact occurs by particle rearrangement, elastic deformation, plastic deformation and particle fragmentation (Mashadi and Newton, 1988). Therefore the 'strength' of the compact depends to some degree on the extent of plasticity of the powder material and the number of contacts between particles. Hence, for materials that undergo little plasticity under the conditions at which these compacts are made, i.e. exhibit brittle behaviour, the powder particles might not adhere so well during the formation of the compact, thereby making it easier to deform. For work-hardening materials increased hardness due to plastic flow adds to the complexity of compacted specimens. The greatest uncertainty surrounding the use of compacted specimens is the difficulty of distinguishing between intrinsic particulate properties from the assembly properties (Kwan et al., 2004). In addition, the correlations used for extrapolation of the data do not account for effects such as binding and size reduction due to fragmentation which can take place during the preparation of the powder compact (Fagan et al., 1996).

Over the past thirty years nano-indentation has been developed enabling indentation testing on individual particles (Arteaga et al., 1993). Nano-indentation involves the use of a three sided pyramidal, diamond indenter with an included angle of 142.3 °, known as a Berkovich indenter. With this tip low loads up to 500 mN can be applied to specimen surfaces, and information such as the elastic modulus, hardness and fracture toughness are evaluated from the indented area using well established methods described by Oliver et al. (1992) and Arteaga et al., 1993. Nano-indentation permits the use of small sizes of particles of about 100 μm, and hence allows the use of batch produced materials, as received, without the need for specially grown crystals which can take a lot of time and effort to prepare. However, mounting micron-sized particles on an anvil in a firm position and presenting a flat surface for testing is still very challenging. According to Dukino and Swain (1992), compared with a Vickers indenter, more exact results can be obtained with the Berkovich tip and at lower loads applied during nano-indentation tests. The small strains accessible through indentation allow for the evaluation of deformation with minimal or no fracture and the relatively small amount of material necessary for indentation is beneficial, as large molecular crystals are difficult to obtain (Ramos and Bahr, 2007). In comparison to the use of compacts, with nano-indentation there is certainty that the single particle and not assembly properties are measured. However, these measured values can only be used with confidence if sample preparation is carried out properly and the measurements are carried out at conditions (depth/load) such that bulk properties and not surface asperities are measured. Oliver et al. (1986) and Arteaga et al. (1993) found that at low penetration depths, the hardness was higher than bulk hardness. Possible reasons given by the above authors for this observation were micro-plastic deformation leading to work-hardening of surface layers, surface chemical effects, skin formed during drying, material property variation with depth and/or surface roughness. Therefore it is important to bear this in mind and identify whether the interest is in the surface or bulk (interior) properties. Tabor (1951) suggested that the effect of roughness on hardness is negligible if the indentation depths are much greater than the surface roughness. Also, polishing has been suggested to reduce the effect of roughness on the results (Bobji and Biswas, 1998). However, this is difficult to carry out on specimens in the micron-sized range. Arteaga et al. (1993) found the hardness values of three types of pure dried vacuumed NaCl salt to decrease with indentation depth up until a point, after which it remained more or less constant. The effect of the applied load on the measured properties of three pharmaceutical compounds

was investigated by Taylor et al. (2004b). While the hardness values of two of the materials tested by these workers were found to be independent of the load applied in the range of 40–80 mN, for the third material both the hardness and Young's modulus were found to decrease at higher loads. Duncan-Hewitt and Weatherly (1989a) suggested that at higher loads extensive crack formation could take place, resulting in a significant reduction of hardness and Young's modulus. On the other hand, at low loads vibrations might prevent the indenter tip maintaining a good contact with the crystals surface thus generating noisy load–displacement plots that would be difficult to analyse (Taylor et al., 2004b). Therefore it is important to determine the variation of these properties with the applied load, and a suitable load/depth chosen. By carrying out indentation tests on a number of materials at the same peak load, Oliver and Pharr (1992) observed that while in some materials (fused silica, sapphire) the displacement during unloading was entirely elastic, for others (such as soda-lime glass and tungsten), it was not. For some materials which are prone to creep i.e. time-dependent plastic deformation if complete plastic flow is not allowed at peak load this could lead to inaccurate values of Young's modulus being obtained from the unloading curve. Introduction of dwell time at peak load can be introduced to diminish this effect. In addition to the aforementioned factors, the mechanical properties of crystalline materials may vary with crystallographic direction depending on the nature of bonding and crystal structure of the solid.

In the study by Elban et al. (1994) loads in the range 0.15–4.9 N were applied successfully onto specially grown sucrose single crystals during indentation, with a dwell time of 20 s. For indentations carried out on freshly cleaved surfaces, a fracture toughness value of 0.055 MPa $m^{1/2}$ was reported for cracks on plane (1 0 0). This value is comparatively lower than the values obtained by Duncan-Hewitt and Weatherly (1989b) who applied maximum loads of 147 mN during indentation of sucrose. The Vickers hardness values of faces (1 0 0), (0 0 1), (0 1 0) and (1 1 0) of sucrose were compared by Duncan-Hewitt and Weatherly (1989b), and the hardness was found to be independent of face and indenter orientation. No occurrences of change in crack length over time were observed and measurement of the fracture toughness of the different planes did not show any appreciable differences in their values suggesting that the fracture behaviour of sucrose is not sensitive to crystallographic direction. When the indenter diagonal was aligned parallel to the lowest index planes, Duncan-Hewitt and Weatherly (1989b) observed cracks on the (1 0 0) plane in the [1 1 0] direction. However, in contradiction to literature (Duncan-Hewitt and Weatherly, 1989a; Ramos and Bahr, 2007; Beevers et al., 1952; Kumaresan and Babu, 1997) that propose the (1 0 0) to be the preferred cleavage plane, and to the work of Elban et al. (1994) which shows the (1 0 0) plane to have the lowest attachment energy, Duncan-Hewitt and Weatherly (1989b) observed the cracks directed along (1 0 0) planes to be shorter or of the same length in comparison to cracks on other planes.

Using a blunted cube corner of effective tip radius 960 nm, Ramos and Bahr (2007) studied the effect of surface and crystal conditions on the habit and freshly cleaved (1 0 0) planes of specially grown and as-received sucrose. They found the values of Young's modulus and hardness to be very similar for both types of crystals with values 33.5 ± 0.7 GPa and 1.62 ± 0.17 GPa, respectively. A comparison of the properties on the (1 0 0) and (0 0 1) planes showed Young's modulus to be anisotropic and hardness to be isotropic. Other observations by these authors include low-load inflection points on the load displacement curve which was attributed to the transition from elastic to plastic deformation. This conclusion seems plausible for tests carried out on freshly cleaved surfaces which are unlikely to have been affected by surface moisture (depending on the time they have been exposed to humidity between cleavage and testing) while for habit planes, low load inflection points could also be due to the breakage of 'skin' on the surface of the crystals. According to Mathlouthi and Reiser (1995), there exists a thin amorphous layer on the surface of crystalline sucrose and the mechanical properties of the amorphous form could differ from that of the crystalline form. The low elastic recovery upon final unloading and the presence of pile-up at indentation sites suggests the presence of plastic deformation mechanisms in sucrose, in contradiction to Thomas and Williams (1967) who stated that molecular crystals contain a low number of dislocations due to their relatively large unit cells and associated large Burgers' vectors for glide dislocations implying tendency for brittle failure. Unlike observations for sucrose by Duncan-Hewitt and Weatherly (1989b), microindentation studies by Prasad et al. (2001) showed the fracture toughness of Paracetamol to vary noticeably with crystallographic direction, with the lowest fracture toughness measured on the (0 1 0) cleavage plane. In addition, when the indentations were carried out on different faces, most of the cracks had the tendency to form parallel to this plane. Attachment energy calculations showed this plane to have the lowest value. However, the trend of attachment energies of the various planes did not completely correlate with the magnitude of fracture toughness values measured. Nevertheless, Paracetamol was shown to have distinct fracture anisotropy. Both studies on Paracetamol and sucrose have highlighted the fracture anisotropy of these materials, a consequence of their molecular packing arrangement. However, the fracture mechanisms were not correlated to macroscopic breakage behaviour. A study in which this was carried out is the recent work of Meier et al. (2009), where the mechanical properties hardness, Young's modulus and fracture toughness of a number of organic crystalline materials determined by nano-indentation were correlated to the fracture propensity under impact loading. The latter was analysed using the model for brittle failure developed by Vogel and Peukert (2003) described below

$$S_b = 1 - \exp\{-f_{Mat} l k (W_{m,kin} - W_{m,min})\} \quad (6)$$

where S_b is the breakage probability, f_{Mat} is the material properties which comprise the effect of particle size, l, and shape on fracture and the resistance of particulate material against the external load, i.e. the specific impact energy $W_{m,kin}$ and $W_{m,min}$ is the amount of energy that a material can take up without fracture. The breakage parameters f_{Mat} and $W_{m,min}$ of materials, including Aspirin, sucrose and ascorbic acid obtained from single particle impact tests, were correlated to their brittleness indices, H/K_c, as derived from their mechanical properties characterised by nano-indentation. The ratio f_{Mat}/ρ, a measure of the resistance of particulate material against fracture in impact comminution, where ρ is the density of the tested materials, was found to vary linearly with $(H/K_c)^{2.5}$ with a correlation coefficient of 0.83, and a correlation with $R^2 = 0.627$ obtained between H/K_c and $xW_{m,min}$. Some of the materials tested, including Aspirin, sucrose and ascorbic acid are known to have cleavage planes, and important information such as the faces and fracture planes for which these values were derived was omitted in the study by Meier and co-workers. The presence of cleavage planes would affect the breakage of such materials under impact loading since these planes represent the "weakest link" in the chain. Therefore, the focus of this present study is to highlight the influence of cleavage planes in a material on its macroscopic breakage behaviour. For this purpose a well-known organic crystalline material, Aspirin, which is known through empirical studies to have a preferred cleavage plane, was chosen for evaluation. In this, Aspirin has been characterised by nano-indentation on the two most morphologically dominant faces (1 0 0) and (0 0 1), with the hardness, Young's modulus and fracture toughness determined. According to the BFDH (Bravais-Friedel-Donnay-Harker) principle, the larger the

interplanar spacing, the more morphologically important the crystal face will be. Where the face with the lowest attachment energy represents the slowest growing face, it will be the major habit face of the crystal and coincide with the major cleavage plane (Roberts et al., 1994). Based on the molecular modelling work by Pencheva (2008) the (1 0 0) plane was shown to have the largest interplanar spacing and lowest attachment energy, followed by the (0 0 1) plane. Osborn et al. (1999) have suggested the (0 0 1) plane to be the preferred slip plane, while others, including Kim et al. (1985) and Li et al. (2006), have stated the (1 0 0) plane to be the preferred cleavage plane. Umeyama et al. (1979) calculated the interaction energies for the (1 0 0) and (0 0 1) faces and concluded the former to be the cleavage plane as it has the smallest attachment energy.

Furthermore, the fracture mechanism of this material is characterised using quasi-static nano-indentation studies and compared to macroscopic fracture behaviour under single impact tests to highlight the influence of cleavage plane in the breakage mechanism under the latter testing conditions.

3. Experimental

3.1. Materials

Aspirin (acetylsalicylic acid, $C_9H_8O_4$, $M = 180.12$) used in this study is classified as grade Purum, Fluka with an assay of ≤99% obtained from Sigma–Aldrich, UK. It occurs in the form of white crystals or as a crystalline powder, with its melting point in the range 135–137 °C, and solubility of 1 g/300 ml of water at 25 °C. Aspirin crystallises in the monoclinic structure $P2_1/c$ with $a = 11.186$ Å, $b = 6.540$ Å, $c = 11.217$ Å and $\beta = 96.07°$. The structure comprises hydrogen bonded pairs of centro symmetric dimers in a tetra-molecular unit cell (Wilson, 2002).

The crystal shape and dissolution behaviour of acetylsalicylic acid to a degree are dependent on the solvent that is used for crystallisation. Aspirin crystals prepared from aromatic, acyclic or chlorinated hydrocarbons appear to be more prismatic and equidimensional compared to those from other solvents such as water and methanol (Meenan, 1997). Crystals prepared from ethanol tend to be small prisms and from water as thin and plate-shaped, while those crystallised from heptane and hexane tend to be more needle-like (Danesh et al., 2000; Watanabe et al., 1982; Glasby and Ridgway, 1986). The morphology of Aspirin predicted by Hammond et al. (2007) revealing a tablet-like morphology with dominant (0 0 1) and (1 0 0) habit planes together with smaller (1 1 0), (0 1 1) and (1 1 1) end-capping facets around the *b*-crystallographic axis is shown in Fig. 1. Crystallisation in polar solvents tends to produce a more plate-like morphology increasing the importance of the hydrophilic (1 0 0) face at the expense of the more hydrophobic (0 0 1) faces (Hammond et al., 2007). This observation of Hammond et al. (2007) is in line with those of Heng et al. (2006) who observed the (0 0 1) to be more hydrophobic than (1 0 0) using sessile drop contact angle measurements. However they found both the (1 0 0) and (0 0 1) faces to be relatively less hydrophilic compared to the (0 1 1) face. An image of the material obtained using a scanning electron microscope (SEM) is also shown in Fig. 1.

3.2. Experimental procedure

3.2.1. Nano-indentation

Nano-indentation measurements were carried out with a Berkovich nano-indenter device manufactured by Micro Materials Ltd., Wrexham. Prior to testing, particles from a batch of commercially produced samples were examined under a microscope, and relatively large and defect free ones with flat uniform surfaces were chosen for testing. This was to prevent cracks and or damages already present within the particles from influencing the results obtained. The particles were tested as received and no preparation of the particle surfaces was carried out. Care was taken to select large particles of at least 300 μm to provide a large enough space for carrying out several indents on the same particle. Individually selected particles were compared against the calculated morphologies of their crystal structure shown in Fig. 1 and oriented to the crystal surface selected for analysis. Subsequently they were mounted onto Scanning Electron Microscopy (SEM) sample stubs using a thin layer of quick-set adhesive (Permabond 102 medium viscosity) such that only the bases of the particles were in contact with the stub. All the nano-indentation studies were conducted at 24 ± 0.1 °C in a temperature controlled chamber. Initially, the loads (and consequently, depths) of the indents were varied using loading/unloading rates of 20 mN/s with a dwell time of 20 s at maximum load in all the tests. Dwell time was introduced in order to allow time-dependent plastic effects to diminish so that the unloading curve would be entirely elastic as suggested by Oliver and Pharr (1992). For statistical reliability, for each face of Aspirin at least 2 particles were tested with at least 20 indentations made on each particle. However, the exact number of indents made on each particle was determined by the size of the crystal face. A distance of 60 μm was maintained between indents to minimise interactions between the elastic and plastic strain fields of neighbouring indents. A schematic showing an example of the map of indentations made on each particle is shown in Fig. 2. The hardness and Young's modulus of the material were obtained using the analysis methods outlined by Arteaga et al. (1993) and Taylor et al. (2004b). After nano-indentation testing, the indented particles and the stub on which they were glued were stored in air tight containers to prevent the interference of moisture with the cracks formed on the surfaces. The samples were coated with a 5 nm thick layer of platinum to allow for electrical conduction, and subsequently subjected to visual examination using a field emission gun scanning electron microscope (FEGSEM) at most 24 h after indentation. This was done to observe the response of each sample to the applied load, observe the crack morphology in relation to crystallographic orientation and to measure the length of the cracks propagated from the indented area. This is necessary in order to estimate the fracture

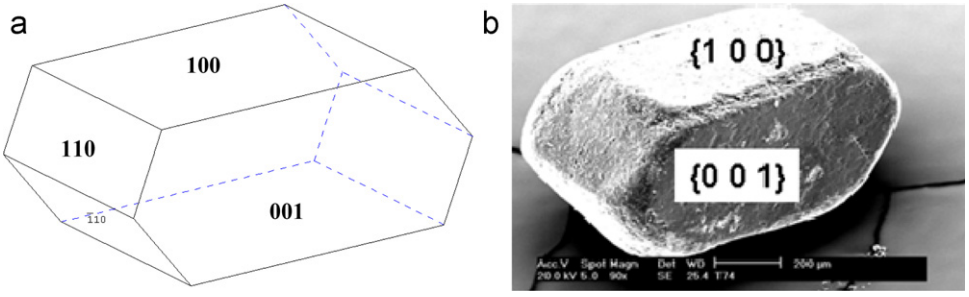

Fig. 1. (a) Morphological sketch of Aspirin drawn using SHAPE and (b) scanning electron micrograph of a representative Aspirin particle.

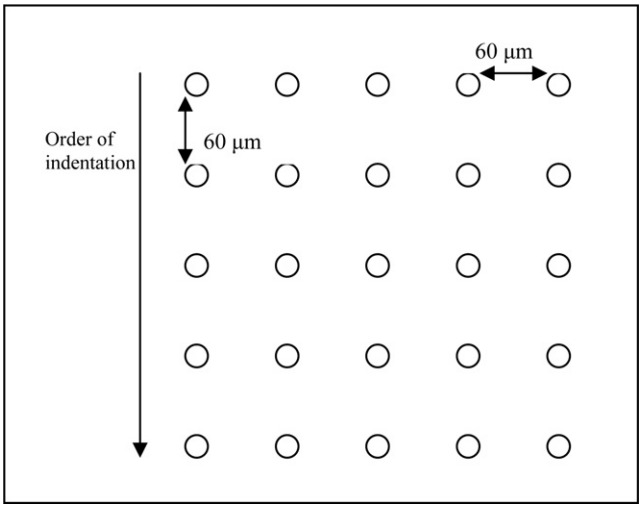

Fig. 2. Schematic showing map of indentations on particles. The actual number of indents made on each particle was dependent on the particle size.

toughness using the equation originally developed by Evans and Wilshaw (1976) and later modified by Dukino and Swain (1992). Details of this approach have been given previously by Arteaga et al. (1993) and Taylor et al. (2004b). Ideally measurement of cracks should be carried out immediately after indentation in case the samples undergo time-dependent, environmentally assisted crack growth as suggested by Ponton and Rawlings (1989) or closing up of the generated cracks over time as observed for citric acid monohydrate by Meier et al. (2009). However this was not feasible given the limited availability of the FEGSEM equipment. Nevertheless, for the material tested here such phenomena have not been previously reported.

3.2.2. Single impact tests

The particles to be tested were first sieved to size ranges, using British Standard sieves BS410. The sieving was performed manually according to the ASTM C136 standards by tapping the sieve and the receiver pan with a wooden stick while rotating the pan and sieve to allow the particles with different orientations to pass through the sieve mesh. Similar to the procedure before nano-indentation, some of the particles in the batch were viewed under the scanning electron microscope (SEM) to make sure they were of good quality. For each test, the sample to be tested in the required sieve cut was weighed to about 2 g in order to keep the test sample amount consistent. Also it was estimated that 2 g of sample contained a sufficiently large number of particles enough to provide statistical reliability of the impact results. The impact test procedure was carried out using an impact test rig based on the work of Yuregir et al. (1986) and described by Bentham et al. (2004). After the impact test, the product was collected with a soft brush and sieved using a sieve two sizes below the original feed size using the procedure outlined by Kwan et al. (2004). The breakage behaviour from single particle impact tests was analysed using the model for the semi-brittle failure of particulate materials developed by Ghadiri and Zhang (2002).

4. Results and discussion

4.1. Analysis of crystal chemistry and molecular packing pattern as a function of crystal orientation

The structure of Aspirin was examined with respect to the approach outlined in Section 2.1. The relative dimensions of the crystallographic cell dimensions together with the inter-molecular

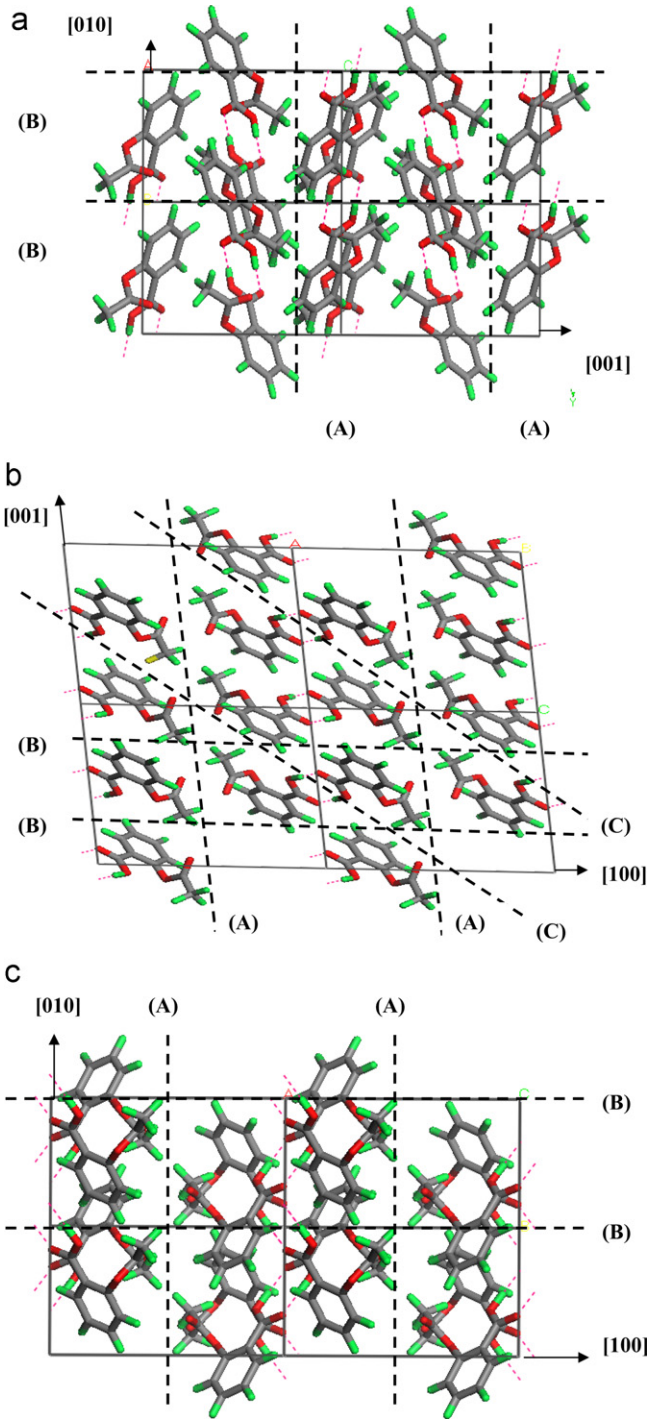

Fig. 3. (a) (1 0 0) projection showing slip possibilities on (0 0 1) (A) planes. Note that slip on (0 1 0) (B) would require breaking the dimer hydrogen bonds. The red and green parts of the molecule represent oxygen and hydrogen, respectively. (b) (0 1 0) projection showing comparatively easy slip possibilities on (1 0 0) (A) crystal planes and less so at (0 0 1) (B). Note that slip on (1 0 1) (c) would involve breaking dimer hydrogen bonds. The red and green parts of the molecule represent oxygen and hydrogen, respectively. (c) (0 0 1) projection showing comparatively easy slip on (1 0 0) (A) planes. Note that slip on (0 1 0) would require breaking the dimer hydrogen bonds. The red and green parts of the molecule represent oxygen and hydrogen, respectively. (For interpretation of the references to color in this figure legend, the reader is referred to the web version of the article.)

packing pattern of acetylsalicylic acid as projected down the three crystallographic axes are shown in Fig. 3(a–c). Analyses suggest that the most likely slip plane would be (1 0 0) followed by (0 0 1). Slip on the (0 1 0) plane would not seem to be very likely given

Table 1
Analysis of the structural factors related to likely slip due to mechanical deformation.

(*h k l*)	Surface[a] Energy (mJ/mm^2)	Slip plane rugosity	Interlocking of slip planes?	Slip system with *b* = [0 1 0]	Slip involving hydrogen bond breaking	Surface cleavage likely?	Plastic deformation likely?
(1 0 0)	(0.0829	Very low	N	Y	N	Y	Y
(0 0 1)	(0.0904	Low	N	Y	N	Y	Y
(0 1 1)	(0.1550	High	Y	N	Y	N	N
(1 1 0)	(0.1430	High	Y	N	Y	N	N
(1 0 1)	N/A	Low	N	Y	Y	N	Possible

[a] Data obtained from Hammond et al. (2006).

that this would involve breaking the dimer hydrogen bonds. Slip on the lower index surfaces such as (1 0 1) plane would also appear to be feasible in terms of the inter-molecular packing but would perhaps be unlikely given that this would require breaking of the dimer bond. This analysis is summarised in Table 1 together with the available calculated values of the surface energies as previously published by Hammond et al. (2006). The likely Burgers' vector for dislocation slip would the shortest axial length [0 1 0], this being the shortest lattice translation, and given that the Bravais lattice is primitive there would be no halving of this distance. Given that the other two lattice constants are nearly twice the magnitude of *b*, it can be speculated that this lattice dislocation would be the most likely and only expected Burgers' vector. Consideration of slip plane and Burgers' vector would suggest that the most likely active slip systems would be (1 0 0) [0 1 0] and (0 0 1) [0 1 0].

4.2. Nano-indentation

4.2.1. Effect of applied load and indentation depth

The variation of the hardness and Young's modulus values with load and depth, and the associated coefficients of variation were used to determine the depth at which the bulk properties could be accurately measured. The load and depth at which the indentations are carried out could be expected to affect the indentation results. At lower loads, the measured values might correspond to the surface properties, which in turn may be affected by surface irregularities and damage during commercial processing. At higher loads, extensive crack formation would be expected to lead to lower values of hardness and Young's modulus (Duncan-Hewitt and Weatherly, 1989a). Also at the high loads a reduction in depth sensitivity may be experienced (Taylor et al., 2004b). Therefore, the measurements should be carried out between the two extremes.

To determine the effect of applied load on indentation depth, the loads were varied from 30 to 120 mN. Five columns of indentations were carried out and different loads were applied to each column. With increased applied load, the depth of the indentation was found to increase as shown in Fig. 4.

To determine the effect of indentation depth on measured values, five to six columns of indentations were made on each particle (see Fig. 5), with each column having a different indentation depth range. The average values of hardness and Young's modulus over each depth range were deduced. The variation of hardness and Young's modulus values of the (0 0 1) face with depth are shown in Figs. 5 and 6, respectively.

From both figures, it is evident that the hardness and Young's modulus decrease gradually with increasing indentation depths even up to depths of 8 μm. This is regarded as the indentation size effect and is expected for soft and crystalline materials (Nix and Gao, 1998). There was no observable transition, such as a sudden large reduction in the hardness or Young's modulus values with increased depth/load which indicated a change from surface mechanical properties to bulk properties, or a transition which marked the onset of significant cracking of the specimen.

Significant differences between surface and bulk mechanical properties measured by nano-indentation could be observed in

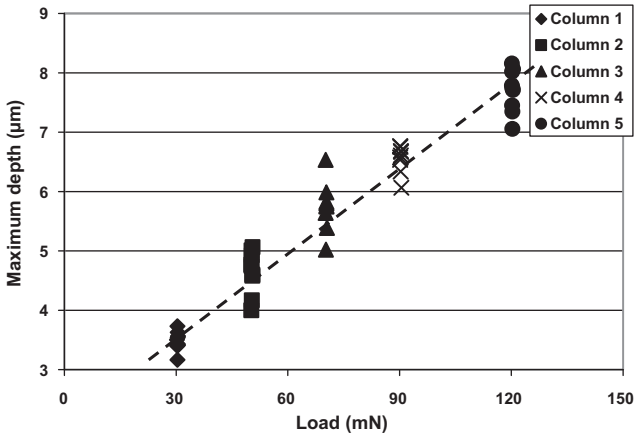

Fig. 4. Variation of depth with increased load for indentations on Aspirin face (0 0 1) at loading rates of 5 mN/s. Each plotting symbol represents a column of indents.

materials, particularly those that undergo work-hardening. Ghadiri et al., 1991 characterised the micro-hardness of industrial grown NaCl crystals from different processing routes, and observed the values measured at a few hundred nano-metres into the crystals to be substantially greater than those measured at several micrometres deep. This was attributed to micro-plastic deformation occurring during 'rough' processing conditions, such that the surfaces of the crystals were work-hardened. For the case of the Aspirin particles tested here, the above observation suggests that this material has not undergone work hardening at the surface and the observed decrease in the hardness and Young's modulus with depth is simply due to indentation size effects.

Another interesting observation as well as the overall reduction of values with increasing depth is that generally the measured values also reduce with increasing indentation depth on each col-

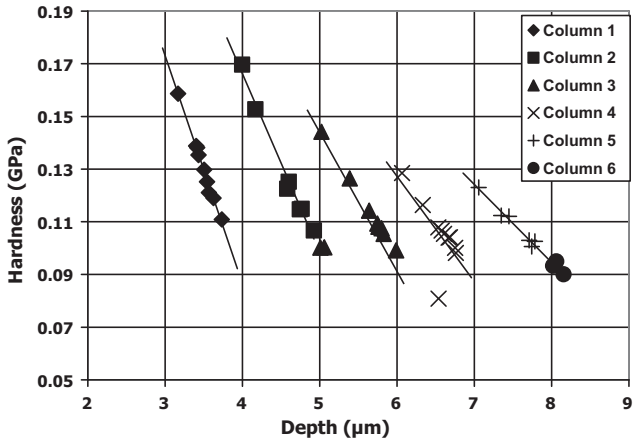

Fig. 5. Variation of hardness with indentation depth on Aspirin face (0 0 1) at loading rates of 5 mN/s for a number of indents spaced 60 μm apart. Each plotting symbol represents a column of indents.

Table 2
Variation of hardness and Young's modulus with indentation depth on Aspirin face (0 0 1) at loading rates of 5 mN/s.

Indentation depth range (μm)	Average hardness (GPa)	CV%	Average Young's modulus (GPa)	CV%
3–4	0.14	13.4	3.11	7.8
4–5	0.12	13.1	2.93	10.0
5–6	0.12	12.6	2.71	5.0
6–7	0.11	11.6	2.81	8.6
7–8	0.11	7.84	2.81	9.3

CV: coefficient of variation.

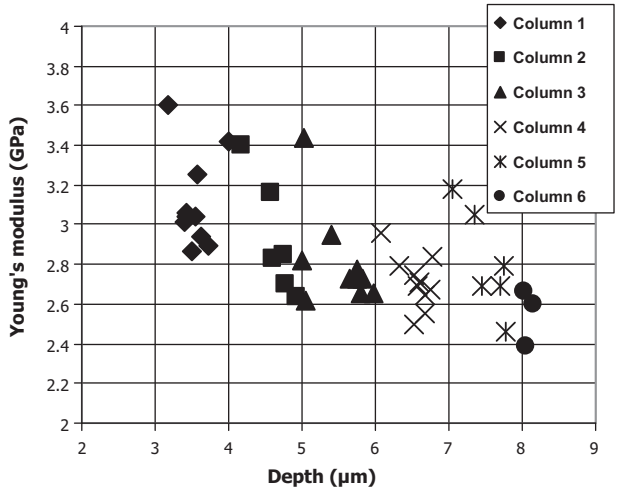

Fig. 6. Variation of Young's modulus with indentation depth on Aspirin face (0 0 1) at loading rates of 5 mN/s spaced 60 μm apart. Each plotting symbol represents a column of indents.

umn. This is most noticeable in Fig. 5 (see trend lines). A possible reason for this observation is that on each column residual elastic strains from each preceding indentation affect subsequent indentations. Averages of the values of hardness and Young's modulus from each depth range are displayed in Table 2. It appears that as the depth increases, the variation of the hardness values is small while Young's modulus decreases up until the range (5–6 μm) and then increases again. Nevertheless, overall the average values do not vary considerably with depth.

The same procedure was repeated for the (1 0 0) face and the variations of hardness and Young's modulus with indentation depth are shown in Figs. 7 and 8, respectively, and summarised in Table 3.

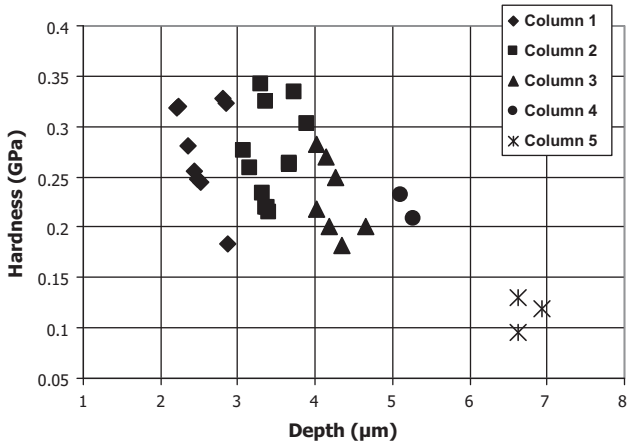

Fig. 7. Variation of hardness with indentation depth on Aspirin face (1 0 0) at loading rates of 5 mN/s spaced 60 μm apart. Each plotting symbol represents a column of indents.

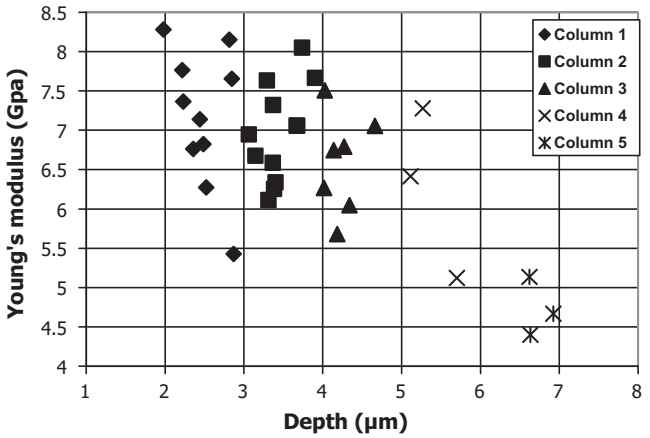

Fig. 8. Variation of Young's modulus with indentation depth on Aspirin face (1 0 0) at loading rates of 5 mN/s spaced 60 μm apart. Each plotting symbol represents a column of indents.

From Fig. 7 at increased depths, i.e. above 6 μm, there is a sudden decrease in the hardness values and this is reflected in Table 3 which shows a sudden decrease of the numerical values of both the hardness and Young's modulus.

Comparing the data for both faces shown in Tables 2 and 3, at depths of about 6 μm, similar hardness values are obtained for both faces. In addition, the coefficients of variation of values across both faces are 15% or lower. Based on these data on the variation of hardness and Young's modulus with depth, the determination of bulk mechanical properties were carried out at depths ~6 μm on both faces. The maximum load was set to 100 mN. The results from these measurements are discussed in the following section.

4.2.2. Indentation load–displacement curves

The load-displacement curve of a material under an applied load gives useful information of its deformation mechanisms under the conditions tested. The indentation load–displacement curves for both faces (1 0 0) and (0 0 1), obtained during analysis of the variation of their mechanical properties with applied load and depth, are shown in Figs. 9 and 10.

For the first comparison, shown in Fig. 9, the minimum and maximum indentation loads were set to 30 and 120 mN, respectively, with no condition set for the depth. Here it can be observed that in order to attain similar indentation depths, loads of up to 70 and 30 mN are needed to be applied on the (1 0 0) and (0 0 1) faces, respectively. Similar observations are made for all the tests carried out on both faces. This observation suggests that plastic flow occurs more readily on the (0 0 1) face compared to the (1 0 0) face.

Fig. 10 shows the comparison of the load–displacement curves obtained from measurements on both faces of Aspirin where the same load is applied to both faces at loading/unloading rates of 20 mN/s. From this, it can be seen that plastic deformation occurs on both faces. However, when the same load is applied on both faces, higher indentation depths are attained on the (0 0 1) face in

Table 3
Variation of hardness and Young's modulus with indentation depth on Aspirin face (1 0 0) at loading rates of 5 mN/s.

Indentation depth range (μm)	Average hardness (GPa)	CV%	Average Young's modulus (GPa)	CV%
2–3	0.28	17.7	7.16	12.3
3–4	0.27	16.9	6.97	8.8
4–5	0.23	15.9	6.59	9.5
5–6	0.22	7.3	6.85	17.3
6–7	0.11	15.5	4.73	7.9

CV: coefficient of variation.

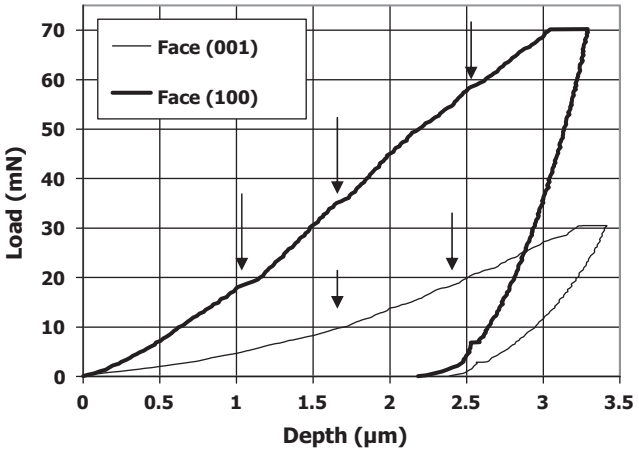

Fig. 9. Load–displacement curves from indentation on faces (0 0 1) and (1 0 0) of Aspirin carried out at loading rates of 5 mN/s and at similar depths. 'Pop-ins' can be observed on both curves, indicated by the arrows.

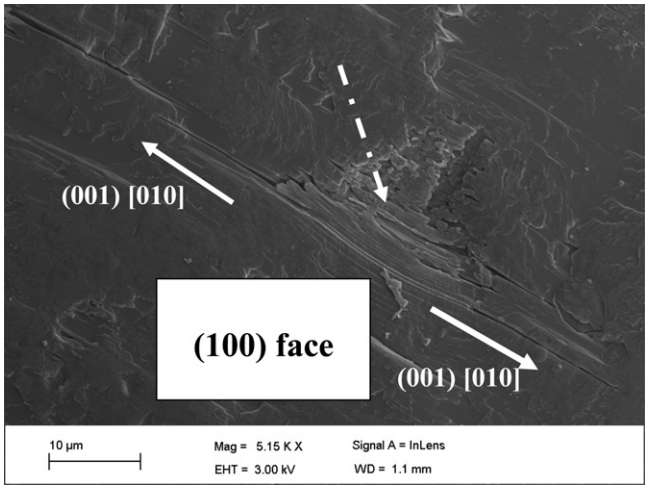

Fig. 11. SEM image of an indent on Aspirin (1 0 0) face.

comparison to the (1 0 0) face. This also indicates that plastic flow occurs more readily on the (0 0 1) face in comparison to the (1 0 0) face.

Another observation from the comparison of these curves is that several 'pop-in' events can be observed along the load–displacement curves of both faces. However, when the same load is applied to achieve similar depths, although both curves show pop-ins (marked by arrows in Fig. 10), they are more frequent and shallow on the (0 0 1) face compared to the (1 0 0) face which shows fewer but deeper 'pop-ins'. This observation of 'pop-ins' at constant load is in line with the observations by Meier et al. (2009) who noticed several 'pop-in' events on the load–displacement curves of indented Aspirin specimens. 'Pop-in' events, i.e. a sudden decrease in hardness at the same load, correspond to sudden cracking of the specimen and/or plastic deformation. These observations are also in agreement with the microindentation tests on single Aspirin crystals carried out by Ridgway et al. (1969) who observed sudden increase in depth without increased loads, even at very low loads.

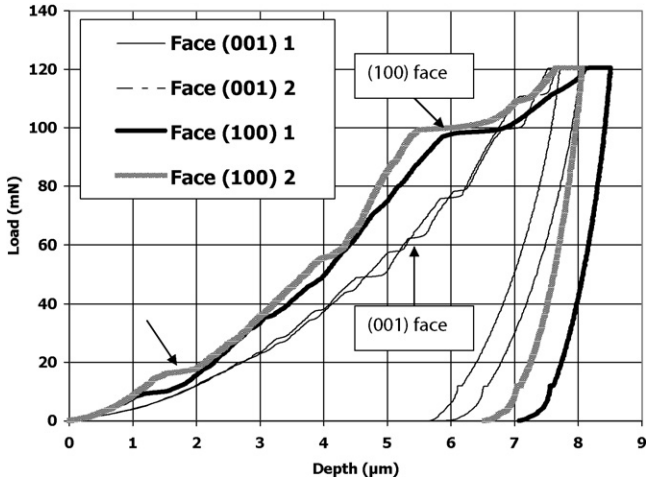

Fig. 10. Load–displacement curves from indentation on (0 0 1) and (1 0 0) faces of Aspirin carried out at loading rates of 20 mN/s, at same load. Pop-ins can be observed on curves produced from both faces.

4.2.3. SEM images of indents

After the determination of the appropriate depth at which the bulk mechanical properties of Aspirin can be measured with confidence, indentation tests were carried out at loading rates of 10 and 20 mN/s. Scanning electron microscopy (SEM) images of the residual indents taken after the indentation tests are shown in Figs. 11–13 for the (1 0 0) and (0 0 1) faces, respectively. On both faces the plastically deformed regions caused by the indentation process can be seen. The cracks propagated from the plastically

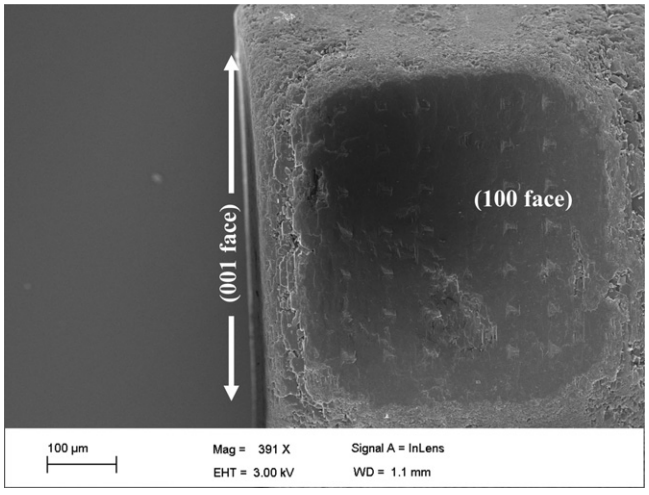

Fig. 12. SEM image of indents on Aspirin face (1 0 0).

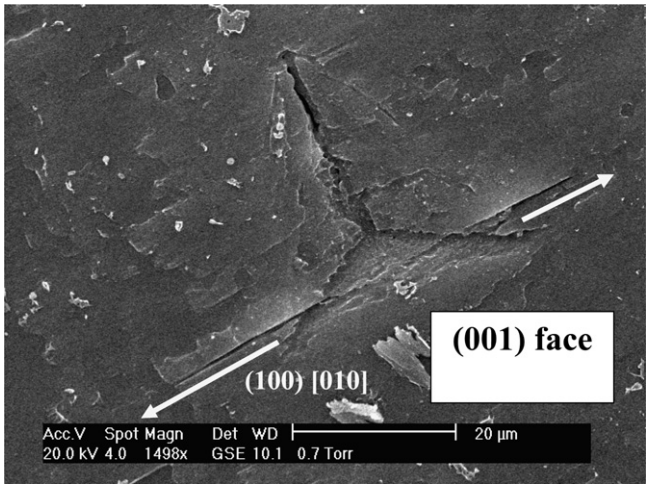

Fig. 13. SEM image of an indent on Aspirin face (0 0 1).

deformed region do not originate from the corner of the indents where the stresses are high, but along specific planes and directions only. For tests carried out on the (0 0 1) and (1 0 0) faces, the cracks are propagated on the (1 0 0) and (0 0 1) planes, respectively, and both in the [0 1 0] direction. The observation of crack propagation only along specific planes is similar across indentations carried out on both faces, and additional images showing this evidence are given in the Appendix A (Figs. A.1–A.4). Crack propagation only along preferential planes is similar to the observations made by Meier et al. (2009) who also carried out nano-indentation tests on Aspirin. These cracks are likely to be cleavage cracks.

While the indents on the (0 0 1) face are very clear, the indents on the (1 0 0) face are found to be less well-defined with the indented area appearing to be somewhat crushed with a step-wise impression directed on the (0 0 1) plane. The reason for this is not clear but it suggests a higher propensity for crack propagation on this plane. There are no apparent differences between the surfaces of the faces which may help to explain the above observation. However, it is worth considering the visual appearance of the residual indents, the stress–strain curves of both faces shown in Fig. 10 and the analysis of crystal chemistry and molecular packing pattern as a function of crystal orientation discussed in Section 4.1 collectively: the planes and direction on which these cracks are propagated coincide with the likely slip systems in this material i.e. (1 0 0) [0 1 0] and (0 0 1) [0 1 0]. Considering the shallow but frequent pop-ins shown on the stress/strain curve of the (0 0 1) face and the comparatively deep but less frequent pop-ins on the load-displacement curves of the (1 0 0) face, it is likely that the pop-ins on the latter are more associated with sudden cracking of the specimen while pop-ins on the former are more as a result of plastic deformation by slip.

The above analyses of the load-displacement curves and the SEM images suggest that crack propagation occurs more readily on the (0 0 1) plane than the (1 0 0) plane, while plastic deformation occurs more readily on the (1 0 0) plane in comparison to the (0 0 1) plane of Aspirin.

4.2.4. Measured mechanical properties

The mechanical properties of Aspirin measured by nano-indentation are shown in Table 4. The hardness values were obtained from the load displacement data of the indentations and Young's moduli of the indentations were calculated from the reduced modulus values also using the method outlined by Oliver and Pharr (1992). The determination of the fracture toughness was carried out by visual analyses of the residual indents and measuring the length of the cracks originated from the plastically deformed region. The final form of the analytical method developed for radial-median crack systems by Evans and Wilshaw (1976) and further modified by Dukino and Swain (1992) for Berkovich indenters was used to determine the fracture toughness values. As shown in the previous section, none of these cracks appeared to be radial cracks, i.e. those propagated from the corners of the indents where the stresses are high but were found to be preferentially aligned along specific crystallographic directions. For Aspirin, highly directional crack systems were observed consistent with strong anisotropy in the mechanical behaviour.

Dukino and Swain (1992) observed that their form of the Evans and Wilshaw (1976) equation, Eq. (7) shown below, although developed for halfpenny crack systems, was also valid for Palmqvist crack systems. Detailed descriptions of both crack systems have been given by Evans and Wilshaw (1976) and Ponton and Rawlings (1989).

$$K_c = x_b \left(\frac{a}{l_i}\right)^{1/2} \left(\frac{E}{H}\right)^{2/3} \frac{P}{c^{3/2}} \quad (7)$$

where x_b is defined as 1.073 x_v, due to the observation made by these workers that cracks from a Berkovich indenter are 1.073 times longer than those generated from Vickers indenters.

A similarity of both crack configurations is that cracks propagate from the elastic–plastic zone beneath the indenter and hence it is likely that Eq. (7) is also valid for crack systems which have this feature but not necessarily having the half penny or Palmqvist shape.

Nevertheless, the use of the Evans and Wilshaw (1976) model is dependent on the fact that the ratio $P/c^{3/2}$ is constant, and as originally applicable to ceramics with a c/a ratio of greater than 2. However the work of Taylor et al. (2004b) highlighted that the relationship between crack length and load still existed even with ratios less than 1.5, indicating that the model does not depend on the ratio of c/a. Nevertheless, in this current study, the average value of c/a for Aspirin was found to be 2.48 ± 0.4 and 2.13 ± 0.2 for measurements on the (1 0 0) and (0 0 1) faces, respectively, thus suggesting the validity of this method of analysis for this material. Furthermore, the value of the ratio of $P/c^{3/2}$ was found to be constant for measurements on both faces of Aspirin; these values for the (1 0 0) and (0 0 1) faces are 0.20 ± 0.05 and 0.32 ± 0.07, respectively. Studies by other authors including Duncan-Hewitt and Weatherly (1989a), Arteaga et al. (1993), Taylor et al. (2004b) and Prasad et al. (2001) have also found this method of analysis of K_c to be suitable for the analysis of pharmaceutical materials. Therefore, Eq. (7) was used here to determine the fracture toughness of Aspirin.

Table 4
Measured mechanical properties of Aspirin determined by nano-indentation.

Indentation face	Fracture plane*	H (GPa)	CV%	E (GPa)	CV%	Elastic Recovery	CV%	K_c (MPa m$^{1/2}$)	CV%
(0 0 1) (1)	(1 0 0)	0.10	10.5	2.96	4.4	0.11	7.5	0.0345	15.5
(0 0 1) (2)	(1 0 0)	0.10	7.9	2.92	4.5	0.11	7.1	0.0344	22.2
(1 0 0) (1)	(0 0 1)	0.12	21.9	5.17	13.9	0.069	9.7	0.0252	32.5
(1 0 0) (2)	(0 0 1)	0.11	22.7	4.86	8.8	0.086	17.9	0.0206	34.4

H (hardness), K_c (fracture toughness), CV (coefficient of variation)

4.2.5. Error analysis

The coefficients of variation of the values are 22% or less with the exception of one set of data. Variation of values across a sample are expected as the contact area between the indenter tip and the sample surface changes from run to run and also due to the high degree of surface roughness associated with bulk manufactured crystals (Meier et al., 2009). While the indents on the (0 0 1) face are very clear, the lack of clarity of the indentations on the (1 0 0) face faces may be responsible for the comparatively high coefficient of variation in the results for measurements on this face as shown in Table 4. Despite this, the hardness values measured on both faces are very similar. In contrast to this, the values of Young's modulus are distinctly different across the two faces. This is in line with observations made for sucrose by Duncan-Hewitt and Weatherly (1989b) and for Paracetamol by Prasad et al. (2001).

The (1 0 0) planes have been suggested to be the preferred cleavage plane by Kim et al. (1985) and Li et al. (2006) with an attachment energy of −18.79 kJ/mol in comparison to that for (0 0 1) which is (41.25 kJ/mol. Considering the surface energy values of the (1 0 0) and (0 0 1) planes reported in Table 1, the values for both faces are very similar (in contrast to attachment energies) suggesting similar propensity for crack propagation after plastic deformation. However, the measured fracture toughness of the (1 0 0) plane is higher than that of the (0 0 1) plane. Therefore a low attachment energy alone is not a sufficiently reliable indication of cleavage plane. This is supported by the analysis of Schultz et al. (1994) who concluded that fracture toughness measurements along different crystallographic directions is the most appropriate method for determining cleavage planes. A comparison of these values to the values obtained by Meier et al. (2009) shows that their measurements of Young's modulus and fracture toughness are more in line with those of this work for the (0 0 1) plane as they obtained values of 5.44 GPa and 0.0211 MPa $m^{1/2}$ respectively, with an error variation of 35.8% for the latter. However, in their study the crystallographic faces on which the indentations were made were not reported. Keeping in mind indentation size effects, the results by Meier et al. (2009) were obtained at a depth range of 1.3–2 μm, while the depth range of 3–6 μm were employed here. In corroboration to the load-displacement curves of both planes and the SEM images of the indents, it is clear that Aspirin has a fracture toughness anisotropy and the propagation of cracks occurs along [0 1 0] directions.

From the analysis of the data, the indentation fracture of Aspirin occurs along the crystallographic planes (1 0 0) and (0 0 1). The fracture toughness of the (0 0 1) plane is distinctly lower than the (1 0 0) plane, while plastic flow occurs more readily on the (1 0 0) plane. The latter conclusion is in agreement with general literature. However, the observed lower fracture toughness of the (0 0 1) plane in comparison to the (1 0 0) plane is in contradiction of literature (Kim et al., 1985; Li et al., 2006) which suggests the (1 0 0) plane to be the cleavage plane. Nevertheless, clear evidence has been presented in this work to support the conclusion that the (0 0 1) plane is the preferred cleavage plane for Aspirin.

4.3. Single particle impact tests

Initially single particle impact tests were carried out in the velocity range between 15 and 35 m/s. Analysis of these data showed that Aspirin undergoes a high extent of breakage of up to 45% in this range. This suggests that the particles readily fragment in addition to chipping under these loading conditions. The analysis model of Ghadiri and Zhang (2002) used here is ideal for this purpose as this was developed specifically for the characterisation of the breakage of materials which undergo damage by chipping in the semi-brittle mode of failure. From previous work by Kwan et al. (2004) and Yang et al. (2007) the chipping mode corresponds to small extents of breakage. The more extensive breakage observed for Aspirin in this study suggests that this model might not be valid for characterisation of the breakage of this material under these conditions. Therefore the tests were repeated at a lower velocity range, where the extent of breakage would be expected to be lower.

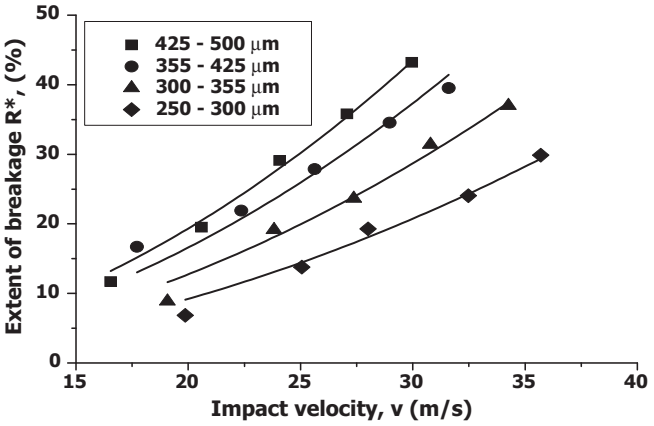

Fig. 14. Extent of breakage of Aspirin with fitting equation of $R^* = C_1 v^2$.

4.3.1. Higher impact velocity range

The results for the high velocity range of Aspirin feed sizes are plotted in Fig. 14. The correlation coefficient (R^2) for these data fitted to Eq. (4) are given in Table 5, where a good agreement with the Ghadiri and Zhang (2002) model is observed.

From Fig. 14, as expected, it can be observed that the extent of breakage of Aspirin particles generally increase with an increase in impact velocity for all the feed sizes tested. The graph also shows an increase in the extent of breakage of the particles with an increase in particle size. The latter is expected to be linear in line with the model of Ghadiri and Zhang (2002). Fig. 14 also includes the power law curve fitting to a power of 2, again in line with the model of Ghadiri and Zhang (2002).

$$R^* = \frac{\alpha_P \rho l H}{K_c^2} v^2 \tag{8}$$

where R^* is the breakage propensity and v is the impact velocity. The group in front of the velocity describes the material properties and are lumped together as C_1 given by:

$$C_1 \frac{\alpha_P \rho H l}{K_c^2} = \alpha_P \rho \left[\frac{H}{K_c^2}\right] l \tag{9}$$

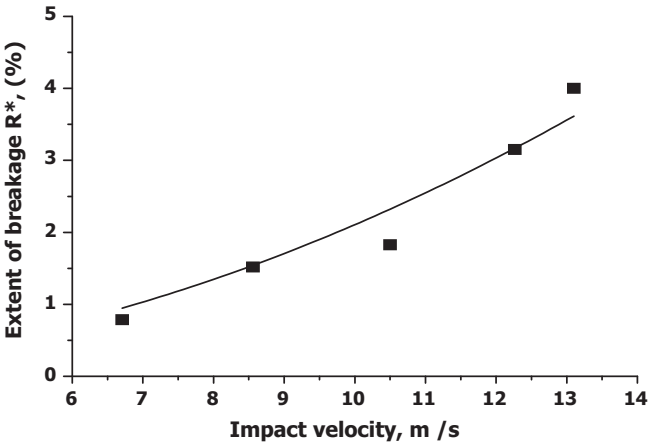

Fig. 15. Impact breakage behaviour of Aspirin at low impact velocities with fitting equation of $R^* = C_1 v^2$ (425–500 μm).

Table 5
Summary of C1 and regression coefficient values of Aspirin from single impact tests in the high velocity range, where $C_1 = (\alpha_P \rho H l/K_c^2)$ as described in Eq. (9).

Size range (μm)	C_1	C_1/l	R^2
425–500	0.0483	104.4	0.993
355–425	0.0415	106.4	0.944
300–355	0.0319	97.4	0.979
250–300	0.0231	84.0	0.977

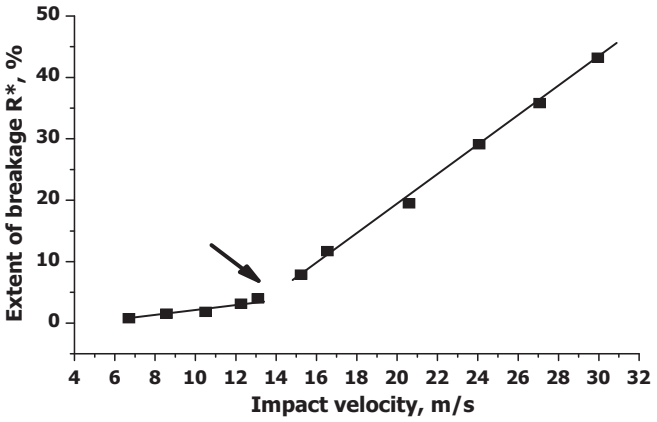

Fig. 16. Full impact breakage behaviour of Aspirin with fitting equation of $R^* = C_1 v^2$.

where α_P is the proportionality constant and represents the influence of the geometry of chipping, ρ is the material density, H is hardness, l is particle size, and K_c is fracture toughness.

It is worth noting that the model of Ghadiri and Zhang (2002) is based on the propagation of lateral cracks from the plastic region while fragmentation occurs by the propagation of radial cracks. Breakage propensities of up to 45% as shown in Fig. 14, and close fitting of the data (the regression coefficients are all well above 0.94) by the Ghadiri and Zhang (2002) model indicates that the fragmentation behaviour of Aspirin is equally well-described by this model. Another point to note for the results given in Table 5 is that the value of C_1 is linearly proportional to particle size (with a coefficient of variation of 4.6) hence the data could be unified by plotting in the form of $v^2 l$.

4.3.2. Lower impact velocity range

The impact tests on Aspirin were repeated at a lower velocity range, 6–14 m/s, where the breakage propensity was relevant to material removal by chipping and this is presented in Fig. 15.

Tests on the effect of particle size were not repeated at these lower velocity ranges because the effect of particle size on breakage propensity has already been demonstrated above. The computed value of C_1 fitted according to Eq. (7) for this data set is also shown here. The data show that the breakage behaviour of Aspirin at lower impact velocities is also well described by the Ghadiri and Zhang (2002) model. At lower impact velocities, the breakage is by chipping as observed by viewing the particles by microscopy, whereas fragmentation occurs at higher impact velocities. Plotting all the data for both velocity ranges on one graph in Fig. 16 shows that the

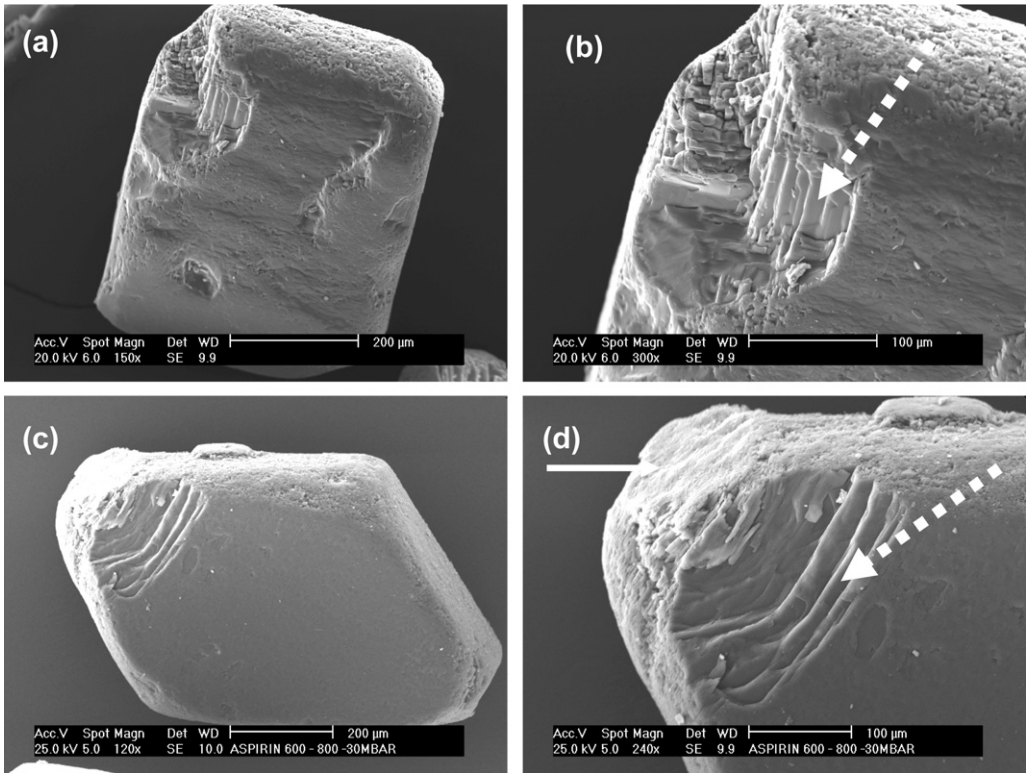

Fig. 17. (a–d) SEM images showing the damage morphology of Aspirin particles after impact at ambient temperature, low impact velocities. (a) and (b): 425–500 μm, 13 m/s, (c) and (d): 600–800 μm, 13 m/s.

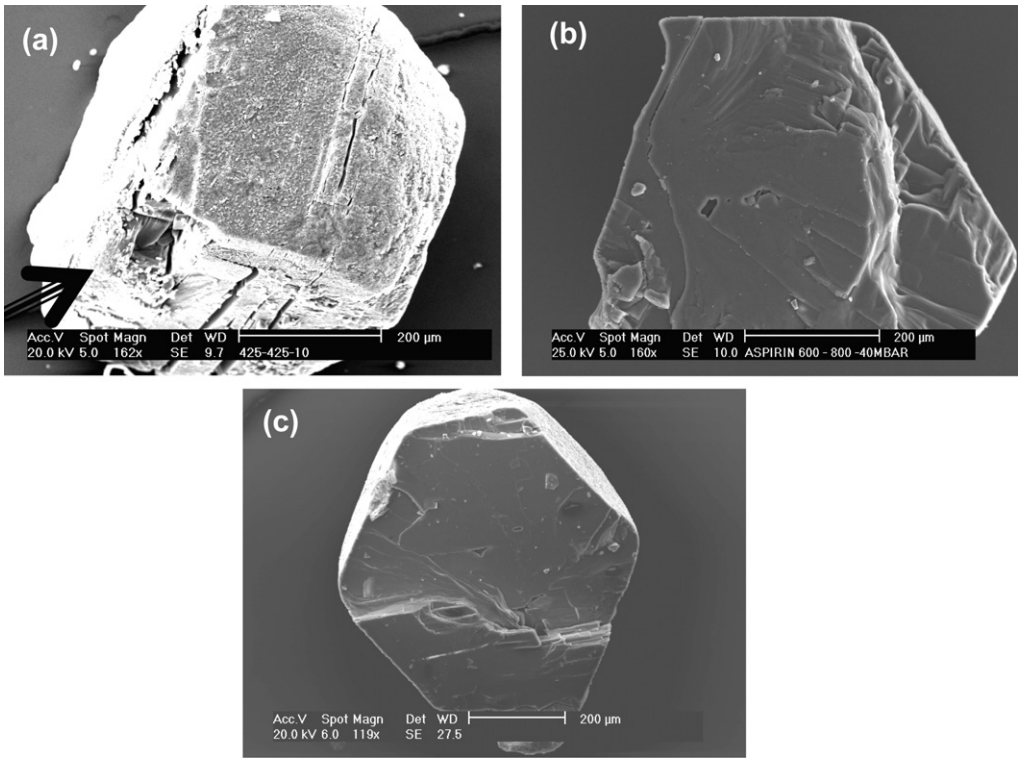

Fig. 18. (a–c) SEM images showing the damage morphology of Aspirin particles after impact at ambient temperature and high impact velocities: (a) 17 m/s, (b) 27 m/s and (c) 27 m/s.

transition zone from primarily chipping to onset of fragmentation lies somewhere between 13 and 15 m/s velocity range.

4.3.3. SEM images of damaged particles

The mother particles collected after the impact tests and visually analysed using scanning electron microscopy are shown in Figs. 17 and 18.

Similar to the propagation of cracks along preferential planes observed from the nano-indentation tests, the impact fracture of Aspirin, shown in Fig. 17(a–d), also shows preferential breakage along specific planes, as demonstrated by the sharp distinctive staircase-like patterns shown by the arrows. This is indicative of the presence of cleavage planes in the crystal structure (Schultz et al., 1994). The particles shown in Fig. 17(c and d) are larger particles of size 600–800 μm, impacted at the same velocity.

The cracks originate from the point of impaction of the particles, indicated by the solid arrow in Fig. 17(d), at the corners and edges. Since Aspirin exhibits preferential cleavage behaviour, it is expected that on impact, following plastic deformation, there is a high probability that the propagation of cracks would occur on the lowest fracture energy planes, which from the previous chapter corresponds to (0 0 1). Images of damaged mother particles of size range 425–800 μm from tests carried out at higher impact velocities from 17 to 27 m/s, are shown in Fig. 18(a–c) below, where evidence of damage along preferential planes is also shown here.

In Fig. 18(a), the point of detachment of a chip can be seen (indicated by the arrow) as well as the propagation of cracks along several planes. Fig. 18(b and c) show Aspirin particles which have been completely split into two and the surfaces of damage are smooth, indicating that fragmentation of Aspirin occurs through preferential cleavage planes.

5. Conclusions

The breakage behaviour of a representative organic molecular material, Aspirin, has been characterised both by quasi-static nano-indentation using a Berkovich indenter, and dynamic impact tests using a single particle impact test rig. The results have shown that the chipping and fragmentation behaviour of Aspirin under impact loading is described well by the Ghadiri and Zhang (2002) model.

Aspirin demonstrates strong anisotropy in its fracture behaviour as cracks originating from plastically deformed regions were found to propagate on preferential cleavage planes. While the hardness was found to be similar on the two faces measured, Young's modulus and fracture toughness measured on the (1 0 0) and (0 0 1) faces were observed to be distinctly different. Analyses of the load–displacement generated during indentation highlighted that plastic flow occurred more readily on the (1 0 0) plane. The fracture toughness of cracks on the (0 0 1) plane was distinctly lower than that of the (1 0 0) plane, indicating that the former is the preferred cleavage plane for Aspirin.

Observations of the damage morphology of the product particles after impact tests are in agreement with the breakage mechanisms observed during nano-indentation studies; the fracture of Aspirin during nano-indentation and single impact occurs on preferential cleavage planes. This is indicated by the propagation of cracks during nano-indentation, and the step-wise detachment of debris in impact chipping as observed by SEM. Hence the presence of cleavage planes is one of the dominant factors in the fracture mechanism of Aspirin under both quasi-static and impact loading conditions, a consequence of the molecular packing pattern dictated by its crystal structure.

Therefore, when nano-indentation is used as a predictive tool for assessing particle breakage mechanisms under impact loading conditions the fracture anisotropy of a material should be considered.

Acknowledgements

The authors gratefully acknowledge financial support from the International Fine Particle Research Institute (IFPRI) and are grateful to Drs Craig Bentham (Pfizer) and Renee Boerefijn (Purac) for their helpful comments and co-ordination of the IFPRI project. Appreciation is due to Toshiko Izumi and Syarifah Abd Rahim of Leeds for the morphological sketch given in Fig. 1(a) and the molecular packing patterns shown in Fig. 2, respectively.

Appendix A. Additional SEM images of indentations on Aspirin

The arrows show cracks in the [0 1 0] direction. For indents on the (0 0 1) and (1 0 0) faces the cracks are propagated on the (1 0 0) and (0 0 1) planes, respectively.

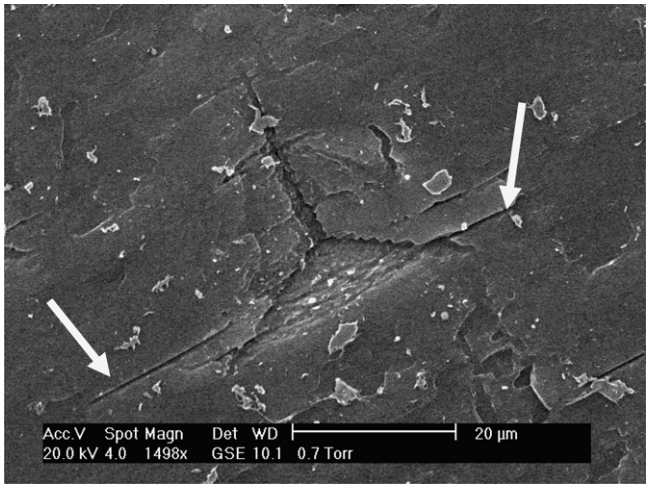

Fig. A.1. SEM image of indentation carried out on face (0 0 1) of Aspirin.

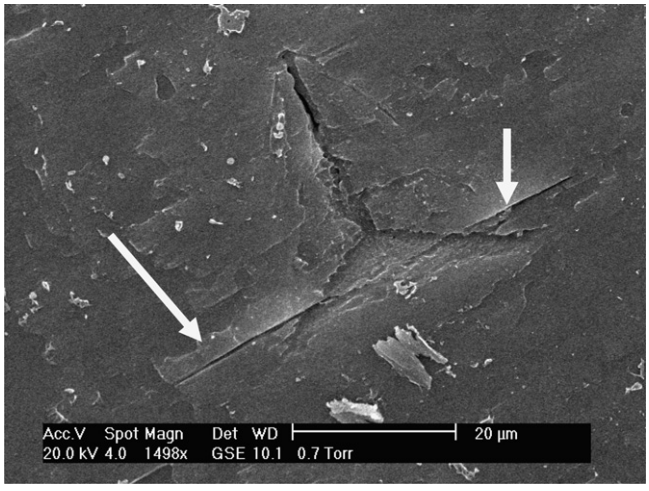

Fig. A.2. SEM image of indentation carried out on face (0 0 1) of Aspirin.

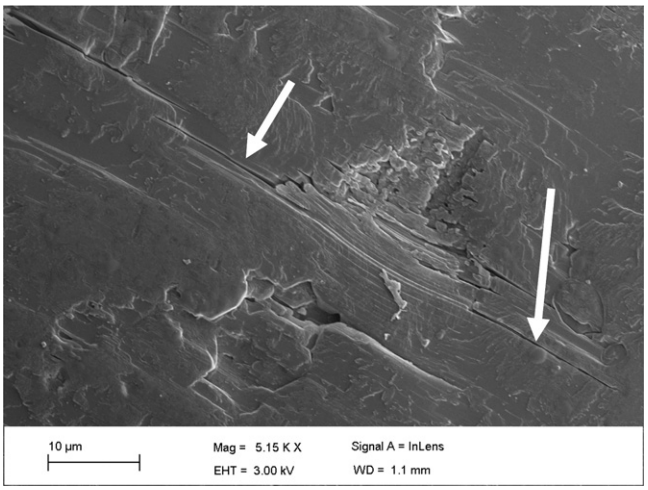

Fig. A.3. SEM image of indentation carried out on face (1 0 0) of Aspirin.

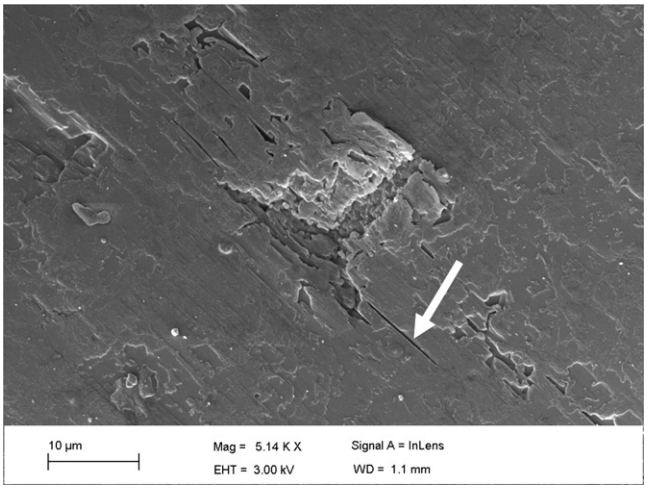

Fig. A.4. SEM image of indentation carried out on face (1 0 0) of Aspirin.

References

Arteaga, P.A., Ghadiri, M., Lawson, N.S., Pollock, H.M., 1993. Use of nanoindentation to assess potential attrition of particulate solids. Tribol. Int. 26, 305–310.
Bassam, F., York, P., Rowe, R.C., Roberts, R.J., 1990. Young's modulus of powders used as pharmaceutical excipients. Int. J. Pharm. 64, 55–60.
Beevers, C.A., McDonald, T.R.R., Robertson, J.H., Stern, F., 1952. The crystal structure of sucrose. Acta Crystallogr. C. 5, 689–690.
Bentham, A.C., Kwan, C.C., Boerefijn, R., Ghadiri, M., 2004. Fluidised-bed jet milling of pharmaceutical powders. Powder Technol. 141, 233–238.
Bobji, M.S., Biswas, S.K., 1998. Estimation of hardness by nano-indentation of rough surfaces. J. Mater. Res. 13 (11), 3227–3233.
Danesh, A., Davies, M.C., Hinder, S.J., Roberts, C.J., Tendler, S.J.B., Williams, P.M., Wilkins, M.J., 2000. Surface characterisation of Aspirin crystal planes by dynamic chemical force microscopy. Anal. Chem. 72, 3419–3422.
Dukino, R.D., Swain, M.V., 1992. Comparative measurement of indentation fracture toughness with Berkovich and Vickers indenters. J. Am. Ceram. Soc. 75 (12), 3299–3304.
Duncan-Hewitt, W.C., Weatherly, G., 1989a. Evaluating the deformation kinetics of sucrose crystals using microindentation techniques. Pharm. Res. 6 (12), 1060–1066.
Duncan-Hewitt, W.C., Weatherly, G., 1989b. Evaluating the fracture toughness of sucrose crystals using microindentation techniques. Pharm. Res. 6 (5), 373–377.
Elban, W.L., Sheen, D.B., Sherwood, J.N., 1994. Vickers hardness testing of sucrose single crystals. J. Cryst. Growth 137 (1–2), 304–308.

Evans, A.G., Wilshaw, T.R., 1976. Quasi-static solid particle damage in brittle solids—1. Observations analysis and implications. Acta Metall. Mater. 24 (10), 939–956.
Fagan, P., Harding, V., Norman, G., Arteaga, P., Ghadiri, M., 1996. Comparative study of the mechanical behaviour of α-lactose from measurements on compacted beam specimens, controlled powder compression and single crystals. Proceedings of 5th World Congress on Chemical Engineering/2nd International Particle Technology Forum, San Diego, pp. 590–595.
Ghadiri, M., Yuregir, K.R., Pollock, H.M., Ross, J.D.J., Rolfe, N.J., 1991. Influence of processing conditions on attrition of NaCl crystals. Powder Technol. 65 (1–3), 311–320.
Ghadiri, M., Zhang, Z., 2002. Impact attrition of particulate solids. Part 1: A theoretical model of chipping. Chem. Eng. Sci. 57, 3659–3669.
Glasby, J., Ridgway, K., 1986. The crystallisation of Aspirin from ethanol. J. Pharm. Pharmacol. 20 (Suppl.), 948–1038.
Hammond, R.B., Pencheva, K., Roberts, K.J., 2006. A structural–kinetic approach to model face-specific solution/crystal surface energy associated with the crystallization of acetyl salicylic acid from supersaturated aqueous/ethanol solution. Cryst. Growth Des. 6, 1324–1334.
Hammond, R.B., Pencheva, K., Ramachandran, V., Roberts, K.J., 2007. Application of grid-based molecular methods for modeling solvent-dependent crystal growth morphology: Aspirin crystallised from aqueous ethanolic solution. Cryst. Growth Des. 7, 1571–1574.
Heng, J., Bismarck, A., Lee, A.F., Wilson, K., Williams, D.R., 2006. Anisotropic surface chemistry of Aspirin crystals. J. Pharm. Sci. 96 (8), 2134–2144.
Hirth, J.P., Lothe, J., 1982. Theory of dislocations, second ed. John Wiley & Sons Inc.
Kerridge, J.C., Newton, J.M., 1986. The determination of the compressive Young's modulus of pharmaceutical materials. J. Pharm. Pharmacol. 38 (Suppl.) 79P.
Kim, Y., Matsumoto, M., Machida, K., 1985. Specific surface energies and dissolution behaviour of Aspirin crystal. Chem. Pharm. Bull. 33, 4125–4131.
Kumaresan, R., Babu, S.M., 1997. Crystal growth and characteristics of sucrose single crystals. Mater. Chem. Phys. 49 (1), 83–86.
Kwan, C.C., Chen, Y., Ding, Y., Papadopoulos, D., Bentham, A.C., Ghadiri, M., 2004. Development of a novel approach towards predicting the milling behaviour of pharmaceutical powders. Eur. J. Pharm. Sci. 23, 327–336.
Lawn, B.R., Marshall, D.B., 1979. Hardness, toughness and brittleness: An indentation analysis. J. Am. Ceram. Soc. 62 (7–8), 347–350.
Li, T., Li, B., Tomassone, M.S., 2006. Surface characterisation of Aspirin crystal planes using molecular dynamics simulations. Chem. Eng. Sci. 61 (15), 5159–5169.
Mashadi, A.M., Newton, J.M., 1988. Determination of the critical stress intensity factor (K_{IC}) of compacted pharmaceutical powders by the double torsion method. J. Pharm. Pharmacol. 40, 597–600.
Mathlouthi, M., Reiser, P., 1995. Sucrose: Properties and Applications. Blackie Academic and Professional, London.
Meenan, P., 1997. Crystal morphology predictive techniques to characterise crystal habit: Application to Aspirin ($C_9H_8O_4$). In: Botsaris, G.D., Toyokura, K., (Eds.), Separation and Purification by Crystallisation. ACS Symposium Series, 667, 2–17.
Meier, M., John, E., Wieckhusen, D., Wirth, W., Peukert, W., 2009. The influence of mechanical properties on impact fracture: Prediction of the milling behaviour of pharmaceutical powders using nano-indentation. Powder Technol. 188 (3), 301–313.
Nix, W.D., Gao, H., 1998. Indentation size effects in crystalline materials: A law for strain gradient plasticity. J. Mech. Phys. Solids. 46 (3), 411–425.
Oliver, W.C., Hutchings, R., Pethica, J.B., 1986. Measurement of hardness at indentation depths as low as 20 nanometres. In: Blau, P.J., Lawn, B.R., (Eds.), Microindentation Techniques in Material Science and Engineering. ASTM STP 889, 90–108.
Oliver, W.C., Pharr, G.M., 1992. An improved technique for determining hardness and elastic modulus using load and displacement sensing indentation experiments. J. Mater. Res. 7 (6), 1564–1583.
Osborn, J.C., York, P., Rowe, R.C., Roberts, R.J., 1999. Prediction of slip planes in molecular crystals by molecular modeling. 14th International Symposium on Industrial Crystallization. Cambridge, United Kingdom, September 12–16, pp. 1166–1174.
Pencheva, K., 2008. Modelling the solid state and surface properties of organic nanosized molecular clusters. Ph.D. Thesis. University of Leeds, U.K.
Ponton, C.B., Rawlings, R.D., 1989. Vickers indentation fracture toughness test—Part 2: Application and critical evaluation of standardised indentation toughness equations. Mater. Sci. Technol. 5, 961–976.
Prasad, K.V.R., Sheen, D.B., Sherwood, J.N., 2001. Fracture property studies of paracetamol single crystals using microindentation techniques. Pharm. Res. 18, 867–872.
Ramos, K.J., Bahr, D.F., 2007. Mechanical behaviour assessment of sucrose using nanoindentation. J. Mater. Res. 22 (7), 2037–2045.
Ridgway, K., Shotton, E., Glasby, J., 1969. The hardness and elastic modulus of some crystalline pharmaceutical materials. J. Pharm. Pharmacol. 21 (Suppl.), 19S–23S.
Roberts, R.J., Rowe, R.C., 1989. Determination of the critical stress intensity factor (K_{IC}) of microcrystalline cellulose using radially edge-cracked tablets. Int. J. Pharm. 52, 213–219.
Roberts, R.J., Rowe, R.C., 1996. The influence of polymorphism on the Young's modulus and yield stress of Carbmarzepine, Sulfathiazole and Sulphanilamide. Int. J. Pharm. 129 (1–2), 79–94.
Roberts, R.J., Rowe, R.C., York, P., 1991. The Relationship between Young's modulus of elasticity of organic solids and their molecular structure. Powder Technol. 65, 139–146.
Roberts, R.J., Rowe, R.C., York, P., 1994. The Poisson's ratio of microcrystalline cellulose. Int. J. Pharm. 105 (1994), 177–180.
Rodford, R.A., Braden, M., Clarke, R.L., 1993. Variation of Young's modulus with the test specimen's aspect ratio. Biomaterials 14 (10), 781–786.
Rowe, R.C., Roberts, R.J., 1996. Mechanical properties. In: Alderborn, G., Nyström, C. (Eds.), Drugs and Pharmaceutical Sciences. Marcel Dekker Inc, New York, pp. 283–321.
Schultz, R.A., Jensen, M.C., Bradt, R.C., 1994. Single crystal cleavage of brittle materials. Int. J. Fracture 65 (4), 291–312.
Tabor, D., 1951. Hardness of Metals. Oxford University Press, Oxford.
Taylor, L.J., Papadopoulos, D.G., Dunn, P.J., Bentham, A.C., Dawson, N.J., Mitchell, J.C., Snowden, M.J., 2004a. Predictive milling of pharmaceutical materials using nanoindentation of single crystals. Org. Process Res. Dev. 8 (4), 674–679.
Taylor, L.J., Papadopoulos, D.G., Dunn, P.J., Bentham, A.C., Mitchell, J.C., Snowden, M.J., 2004b. Mechanical characterisation of powders using nanoindentation. Powder Technol. 143–144, 179–185.
Thomas, J.M., Williams, J.O., 1967. Lattice imperfections in organic solids, Part 2—sucrose. Trans. Faraday Soc. 63, 1922–1928.
Umeyama, H., Nakagawa, S., Moriguchi, I., 1979. Molecular orbital study of the cleavage planes of Aspirin crystals. J. Phys. Chem. 83 (15), 2048–2052.
Vogel, L., Peukert, W., 2003. Breakage behaviour of different materials-construction of a mastercurve for the breakage probability. Powder Technol. 129, 101–110.
Watanabe, A., Yamaoka, Y., Takada, K., 1982. Crystal habits and dissolution behaviour of Aspirin. Chem. Pharm. Bull. 30, 2958–2963.
Wilson, C.C., 2002. Interesting proton behaviour in molecular structures. Variable temperature neutron diffraction and ab initio study of acetylsalicylic acid: characterising librational motions and comparing protons in different hydrogen bonding potentials. New J. Chem. 26, 1733–1739.
Yang, W., Kwan, C.C., Ding, Y., Ghadiri, M., Roberts, K.J., 2007. Milling of sucrose. Powder Technol. 174 (1–2), 14–17.
York, P., Bassam, F., Roberts, R.J., Rowe, R.C., 1990. Fracture mechanics of microcrystalline cellulose powders. Int. J. Pharm. 66, 143–148.
Yuregir, K.R., Ghadiri, M., Clift, R., 1986. Observations on impact attrition of granular solids. Powder Technol. 49 (1), 53–57.